Redox and Catalytic Properties of Copper Molybdates with Various Composition[1]

E. V. Soltys*, Kh. Kh. Urazov, T. S. Kharlamova, and O. V. Vodyankina

Tomsk State University, Tomsk, 634050 Russia
*e-mail: evgenia.soltys@mail.ru
Received January 25, 2017

Abstract—Using XRD and temperature-programmed reduction (TPR), phase and structural transformations of copper molybdates $Cu_3Mo_2O_9$ and $CuMoO_4$ were investigated in the course of their treatment with hydrogen, carbon monoxide or soot. The catalytic properties of copper molybdates $Cu_3Mo_2O_9$ and $CuMoO_4$ were studied in model oxidation reactions of carbon monoxide and soot. Phase and structural transformations of the molybdates, in particular formation of $Cu_{4-x}Mo_3O_{12}$ and $Cu_6Mo_5O_{18}$ phases, was shown to have a significant impact on the formation of active state of the catalysts in the model reactions considered.

Copper and molybdenum oxides are widely used as heterogeneous catalysts for redox reactions in many areas of industry and environmental protection, including water-gas shift reaction [1], soot combustion [2−5], VOCs oxidation [6], synthesis of methanol and higher alcohols [7], oxidation and dehydrogenation of alcohols [8, 9], olefin metathesis [10−12], oxidative cracking of hexane [13, 14], styrene selective epoxidation [15, 16], and others. In some cases, for example, $(CH_3)_2S_2$ oxidation and selective catalytic reduction of NO_x by ammonia, the use of a combination of copper and molybdenum oxides leads to substantial improvement of catalyst properties in comparison with those of individual oxides. This is related to the formation of copper molybdates $Cu_3Mo_2O_9$ and $CuMoO_4$ on the surface of multicomponent catalysts [6, 17−20]. Mixed copper(II) and molybdenum oxides also showed higher catalytic activity in oxidation of soot [21−26], propylene and butylenes [27−31].

The investigation of phase composition of catalysts based on $CuMoO_4$ at different stages of soot combustion [23, 25, 26] and watergas shift reaction [32] showed that the active state of catalyst can significantly differ from the initial one. For soot combustion, the formation of copper(I) molybdates as well as mixed copper molybdate $Cu_{4-x}Mo_3O_{12}$, which is considered the most active phase initiating the catalytic soot combustion, on the surface of $CuMoO_4$ was detected under reaction conditions [23]. A study of

catalysts based on $CuMoO_4$ in water-gas shift reaction by synchrotron-based in situ time-resolved X-ray diffraction and XANES spectroscopy showed that the highest catalytic activity of the catalyst is provided by MoO_2-supported Cu clusters formed during the preliminary reduction of the initial $CuMoO_4$ by hydrogen, while $CuMoO_4$ as well as $Cu_6Mo_4O_{15}$ produced in the course of its reduction under reaction atmosphere is characterized by low catalytic activity [32].

At the same time, the redox properties of copper molybdates of various composition remain poorly studied. In contrast to $CuMoO_4$, there are no studies in literature that describe the phase and structural transformations of $Cu_3Mo_2O_9$ under the redox reaction medium. The phase transformations of $CuMoO_4$ and $Cu_3Mo_2O_9$ during their reduction by hydrogen (27−33 Torr) under static conditions with recirculation in the isothermal regime in the temperature range of 400−500°C were reported in [33], where the reduction of copper(II) molybdates by hydrogen was indicated to occur through a series of consequent transformations. In case of $Cu_3Mo_2O_9$, these depend on the process temperature. $Cu_3Mo_2O_9$ and $CuMoO_4$ are reduced to Cu and MoO_2 with an intermediate formation of $Cu_6Mo_4O_{15}$ phase (or, according to [34], $Cu_6Mo_5O_{18}$) and a mixture of $Cu_6Mo_4O_{15}$ and $Cu_2Mo_3O_{10}$ phases, respectively, under experimental conditions at temperatures below 460°C. The reduction of $Cu_3Mo_2O_9$ is accompanied by formation of $Cu_{4-x}Mo_3O_{12}$ phase at temperatures above 460°C, which from the authors' point of view is connected with the incongruent melt-

---

[1] The article was translated by the authors.

ing of $Cu_6Mo_4O_{15}$ phase. In contrast, the $Cu_{4-x}Mo_3O_{12}$ phase is not formed during the $CuMoO_4$ reduction at temperatures above 460°C despite the presence of the $Cu_6Mo_5O_{18}$ phase in the reduction products. Therefore, the dependence of the phase composition of $Cu_3Mo_2O_9$ reduction products on the process temperature observed in [33] can be due to high rate of reduction of $Cu_{4-x}Mo_3O_{12}$ intermediate produced at 400−460°C and the diffusion limitations of the reduction process above 460°C, rather than the incongruent melting of $Cu_6Mo_5O_{18}$ phase. The regularities of reduction of copper molybdates at temperatures below 400°C, which are of interest for understanding of the mechanism of formation of active state of catalysts operating at low temperatures [6, 17−20], were not considered in [33].

The partial reduction of $CuMoO_4$ during the preliminary treatment of the catalyst in a stream of pure hydrogen at 260°C with the formation of Cu and amorphous MoO_2 on the surface of the initial copper molybdate particles was reported in [32]. However, the use of pure hydrogen for the catalyst reduction is limited by hydrogenation processes and can lead to strong heating and sintering of the reduced sample or active component. In most cases, the formation of the catalyst is carried out under milder reducing conditions with a nitrogen-hydrogen mixture, reformed and furnace gases (containing CO, H_2, CH_4, N_2) or directly under the reaction conditions.

There is also no data on the comparison between the reactivity of simple and mixed oxides based on molybdenum and copper in various redox atmospheres under competitive conditions in the literature. Available studies do not allow making a correct comparison because of different experimental conditions.

Thus, the systematic studies on phase and structural transformations of mixed molybdenum and copper oxides $Cu_3Mo_2O_9$ and $CuMoO_4$ in various redox atmospheres coupled with the results of studies of their catalytic properties in model reactions will allow revealing the features of formation of the active state of multicomponent catalysts on the basis thereof for a series of redox processes.

EXPERIMENTAL

Catalysts Preparation

Copper molybdate with molar ratio of Cu : Mo = 3 : 2 was prepared by co-precipitation method, while copper molybdate with molar ratio of Cu : Mo = 1 : 1 was prepared using sol−gel technique. Ammonium heptamolybdate $(NH_4)_6Mo_7O_{24} \cdot 4H_2O$ and copper nitrate $Cu(NO_3)_2 \cdot 3H_2O$ were used as precursors in both cases.

To prepare the sample with a molar ratio of Cu : Mo = 3 : 2, aqueous solutions of copper and molybdenum precursors mixed in a desired ratio followed by dropwise addition of 0.1 M NaOH as a precipitator to the received solution. The suspension obtained was aged in a mother solution at 60°C for 1 h with continual stirring. The precipitate formed was washed with distilled water. Then, the precipitate was dried at 50°C for 12 h and calcined at 500°C for 4 h.

To prepare the sample with a molar ratio of Cu : Mo = 1 : 1, citric acid was added to aqueous equimolar solution of ammonium molybdate and copper nitrate at the ratio cation : citric acid = 3 : 1; pH 1 was adjusted with NH_4OH solution. The reaction mixture was heated at 80°C with continual stirring until a gel was formed. The gel obtained was dried at 120°C for 24 h, precalcined at 300°C for 12 h and then calcined at 500°C for 24 h.

Individual oxides of molybdenum and copper were prepared by thermal decomposition of ammonium heptamolybdate $(NH_4)_6Mo_7O_{24} \cdot 4H_2O$ and copper nitrate $Cu(NO_3)_2 \cdot 3H_2O$ at 500°C, respectively. The samples obtained were single-phase MoO_3 ($S_d = 3.5$ m^2/g) and CuO ($S_d = 0.2$ m^2/g).

Catalyst Characterization

The phase composition of the samples, both as-prepared and those after various treatments, was studied by X-ray diffraction (XRD) using MiniFlex 600 (Rigaku, Japan) diffractometer with monochromatic CuK_α radiation ($\lambda = 1.5418$ Å). Recording conditions: scanning speed 2°C/min, voltage 40 kV, current 15 mA, the angular range $2\theta = 10°−60°$. The obtained XRD patterns were analyzed with PCPDFWIN database.

Temperature-programmed reduction by hydrogen (TPR-H_2), carbon monoxide (TPR-CO) and carbon (TPR-C) was carried out using the chemisorption analyzer Chemisorb 2750 (Micromeritics, USA) with a thermal conductivity detector in a 20 mL/min flow of 10 vol % H_2 in argon, 5 vol % CO in helium and nitrogen ("high-purity"), respectively. The heating rate was 5°C/min in all cases; additional studies were carried out at a heating rate of 10°C/min for TPR-C. For TPR-C, the samples were mixed with model soot (Carbon Black, Micromeritics) in a weight ratio of 20 : 1. Prior to TPR-H_2 and TPR-CO experiments, the fresh samples were oxidized in a flow of air (20 mL/min) under temperature-programmed oxidation (TPO) mode at a heating rate of 10°C/min to 500°C followed by holding at 500°C for 30 min. To determine the amount of hydrogen consumed during the reduction of copper molybdates, a calibration of the thermal conductivity detector was carried out using standard Ag_2O sample (Micromeritics).

The catalytic activity of copper molybdates was studied in model reactions of CO and soot oxidation. CO was oxidized in the temperature-programmed reaction (TPR) mode using chemisorption analyzer Chemisorb 2750 (Micromeritics) with a thermal conductivity detector and a conjugated quadrupole mass

Table 1. The amount of hydrogen consumed during the reduction of copper molybdates $Cu_3Mo_2O_9$ and $CuMoO_4$ (according to TPR-H_2 and theoretical calculations) as well as the phase composition of the samples reduced to the specified temperature (T)

Sample	T_{peak}, °C	Hydrogen consumption, mmol/g		Reduction	
		experemet	calculation	T, °C	phase composition
$Cu_3Mo_2O_9$	313, 333	3.46 (0.86, 2.60)*	3.41	340	$Cu_6Mo_5O_{18}$, Cu
	380	5.97	6.06	500	Cu, MoO_2
$CuMoO_4$	460	2.02*	2.23	430	$CuMoO_4$, $Cu_6Mo_5O_{18}$, MoO_3
	491	7.37*	6.70	600	Cu, MoO_2
CuO	325	12.53	12.50	500	Cu
MoO_3	725, 787	7.03	6.94	800	MoO_2

* The amount of consumed hydrogen was determined from the area of the peak obtained as a result of deconvolution of the TPR profile.

spectrometer UGA-300 (Stanford Research Systems, USA) using a gas mixture of 1 vol % CO and 1 vol % O_2 in helium in the temperature range from 25 to 500°C and at a heating rate of 5°C/min. Prior to the experiment, a standard oxidative treatment of sample was performed in air (20 mL/min) in the TPO mode at a heating rate of 10°C/min to up to 500°C followed by holding at 500°C for 30 min.

The activity of copper molybdates was studied in the soot oxidation using a synchronous thermal analyzer STA 449 F1 Jupiter (NETZSCH, Germany). The sample mixed with model soot with a weight ratio of 20 : 1 was placed in an alumina crucible and treated under argon (20 mL/min) and air (50 mL/min) atmosphere in the range from 50 to 800°C at a heating rate of 10°C/min. Heat fluxes and mass changes were measured as well as gases evolved were analyzed with a coupled quadrupole mass spectrometer QMS 403 D Aёolos ("NETZSCH") during the experiment. The data obtained were processed using the NETZSCH Proteus® Software. The soot oxidation was further studied in the TPR mode in a flow (20 mL/min) of 10 vol % O_2 in helium at a heating rate of 10°C/min using the chemisorption analyzer Chemisorb 2750 with a thermal conductivity detector and a conjugated quadrupole mass spectrometer UGA-300. The weight ratio of the sample to the soot was also 20 : 1.

RESULTS AND DISCUSSION

Structure of Initial Samples

According to the XRD data, the prepared samples are single-phase, characterized by different composition and structure, and correspond to the orthorhombic $Cu_3Mo_2O_9$ and triclinic $CuMoO_4$ (Fig. 1). The structure of the triclinic copper molybdate $CuMoO_4$ is characterized by the presence of copper in the distorted octahedra CuO_6 and pyramids CuO_5 and molybdenum in a regular tetrahedra MoO_4 [36]. Cop-per-oxygen polyhedra CuO_6 and CuO_5 are connected by an edge forming spiral fragments from five copper polyhedra connected by MoO_4 tetrahedra. The structure of orthorhombic copper molybdate $Cu_3Mo_2O_9$ is also characterized by the presence of copper in distorted octahedra CuO_6 and pyramids CuO_5, forming zigzagging chains of Cu_4O_4 [37, 38]. Molybdenum atoms in MoO_4 tetrahedra link chains of Cu_4O_4 through the total oxygen at the top of polyhedra.

According to the data of low-temperature nitrogen adsorption, the samples of copper molybdates are characterized by low specific surface area: 2.5 m²/g for $Cu_3Mo_2O_9$ and 1.2 m²/g for $CuMoO_4$.

Temperature-Programmed Reduction by H_2

The TPR-H_2 profiles of copper molybdates are shown in Fig. 2a. The reduction profiles of individual CuO and MoO_3 oxides were also presented in the figure for comparison. The reduction of $Cu_3Mo_2O_9$ by hydrogen occurs at relatively low temperatures in the range of 280–420°C. The sample $CuMoO_4$ is reduced at higher temperatures in the range of 400–520°C. The TPR-H_2 profiles of both copper molybdates are characterized by the presence of several peaks of hydrogen consumption, which indicates its stepwise reduction. The phase and structural transformations of copper molybdates during their reduction were studied according to the data of the quantitative calculation of the consumed hydrogen (Table 1) and XRD data of the reduced samples (Fig. 1).

The reduction profile of the $Cu_3Mo_2O_9$ sample is characterized by two clearly distinguishable regions of hydrogen consumption at 280–350°C and 350–420°C. The amount of hydrogen consumed in the low-temperature region in the range of 280–350°C corresponds to the reduction of the initial sample with the formation of copper(I) molybdate $Cu_6Mo_5O_{18}$ and evolution of a part of copper as metallic Cu:

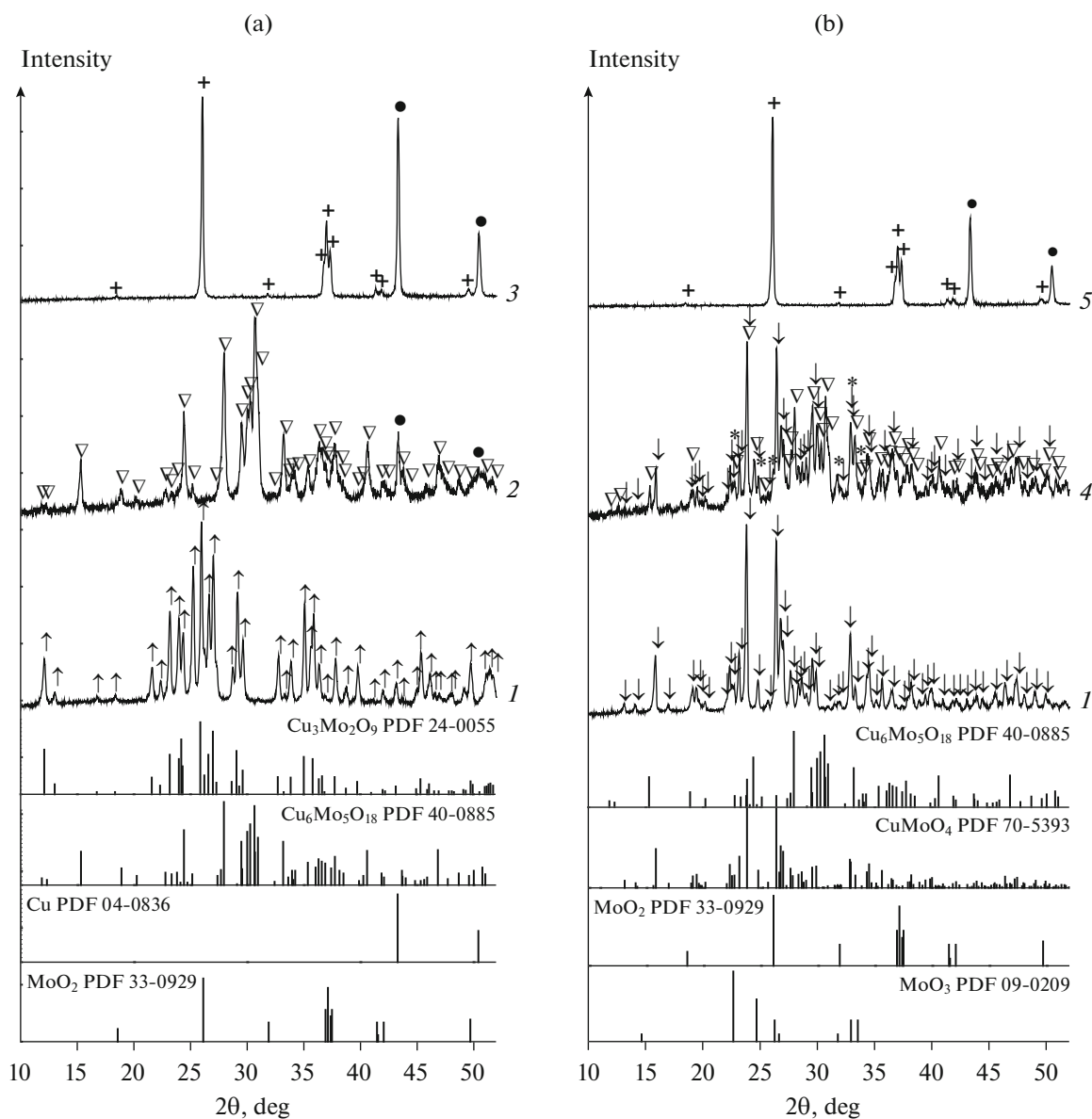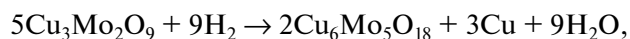**Fig. 1.** X-ray patterns of $Cu_3Mo_2O_9$ (a) and $CuMoO_4$ (b) samples, initial (*1*) and reduced in the course of TPR-H_2 to 340 (*2*), 500 (*3*), 491 (*4*) and 600°C (*5*), and also line-diagrams of phases identified (($\uparrow$) $Cu_3Mo_2O_9$, ($\downarrow$) $CuMoO_4$, ($\bullet$) Cu, (+) MoO_2, ($\triangledown$) $Cu_6Mo_5O_{18}$, (*) MoO_3).

$$5Cu_3Mo_2O_9 + 9H_2 \rightarrow 2Cu_6Mo_5O_{18} + 3Cu + 9H_2O,$$

which is confirmed by the XRD data (Fig. 1a). The hydrogen consumption at higher temperatures in the range 350−420°C corresponds to the reduction of $Cu_6Mo_5O_{18}$ to metallic copper Cu and molybdenum oxide MoO_2.

A detailed analysis of the hydrogen consumption profile in the temperature range from 280 to 370°C shows that it can be represented by two peaks with maxima at 313 and 333°C (see Table 1) indicating that the reduction of $Cu_3Mo_2O_9$ to $Cu_6Mo_5O_{18}$ occurs through several steps. A small peak at 313°C was related to partial reduction of Cu(II) in the initial sam-

ple with the formation of mixed copper molybdate that was generally described in the literature as $Cu_{4-x}Mo_3O_{12}$. The corresponding phase was not detected by off-line XRD due to its rapid subsequent reduction under experimental conditions. The composition of the formed phase was estimated on the basis of the quantitative TPR data taking into account the deconvolution of the TPR profile and assuming the reduction of a part of Cu(II) to Cu(I) [39].

According to estimates made from the TPR-H_2 data, the degree of reduction of Cu(II) present in the sample to the Cu(I) is 31%. This corresponds to partial reduction of the sample to form a mixed copper
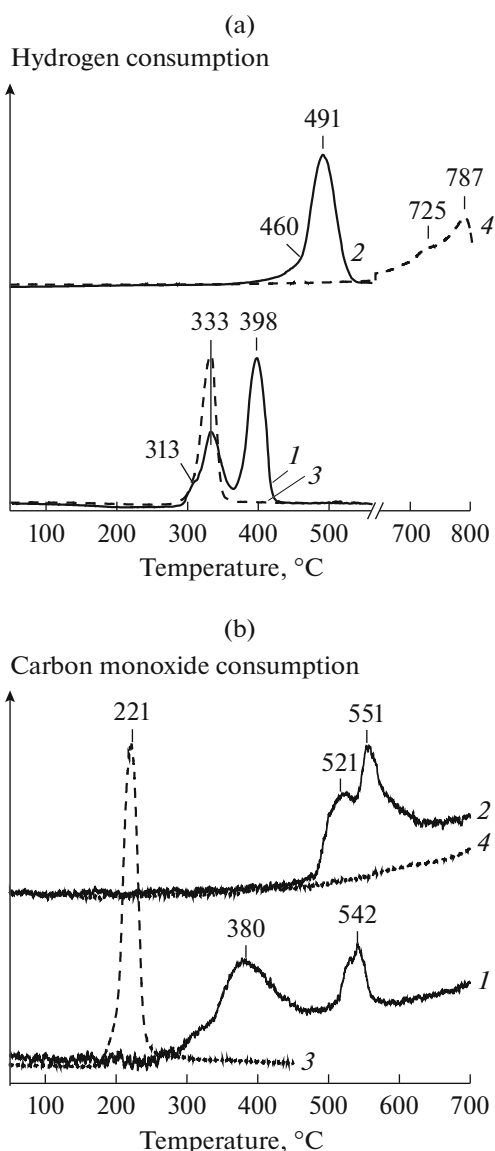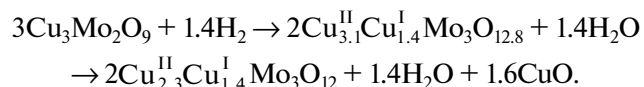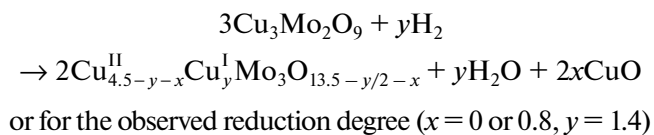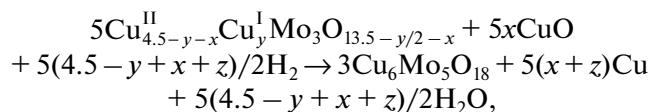
(a)

Hydrogen consumption

(b)

Carbon monoxide consumption

Fig. 2. The TPR-H_2 (a) and TPR-CO (b) profiles of $Cu_3Mo_2O_9$ (*1*), $CuMoO_4$ (*2*), CuO (*3*) and MoO_3 (*4*) samples.

molybdate $Cu_{3.1}^{II}Cu_{1.4}^{I}Mo_3O_{12.8}$, which is not stoichiometric towards oxygen, due to an excessive copper content, or a mixture of oxygen-stoichiometric copper molybdate $Cu_{2.3}^{II}Cu_{1.4}^{I}Mo_3O_{12}$ and copper oxide CuO formed as a result of the segregation of copper excess, which is most probable given the existence region of $Cu_{4-x}Mo_3O_{12}$ [40–43]:

$$3Cu_3Mo_2O_9 + yH_2$$
$$\rightarrow 2Cu_{4.5-y-x}^{II}Cu_y^{I}Mo_3O_{13.5-y/2-x} + yH_2O + 2xCuO$$

or for the observed reduction degree ($x = 0$ or 0.8, $y = 1.4$)

$$3Cu_3Mo_2O_9 + 1.4H_2 \rightarrow 2Cu_{3.1}^{II}Cu_{1.4}^{I}Mo_3O_{12.8} + 1.4H_2O$$
$$\rightarrow 2Cu_{2.3}^{II}Cu_{1.4}^{I}Mo_3O_{12} + 1.4H_2O + 1.6CuO.$$

Subsequent consumption of hydrogen in the region of 318–350°C, described by the peak at 333°C, corresponds to the reduction of the formed mixed copper molybdate or the mixture of $Cu_{4-x}Mo_3O_{12}$ and CuO to form copper(I) molybdate $Cu_6Mo_5O_{18}$ and Cu:

$$5Cu_{4.5-y-x}^{II}Cu_y^{I}Mo_3O_{13.5-y/2-x} + 5xCuO$$
$$+ 5(4.5-y+x+z)/2H_2 \rightarrow 3Cu_6Mo_5O_{18} + 5(x+z)Cu$$
$$+ 5(4.5-y+x+z)/2H_2O,$$

or for the observed reduction degree ($x = 0$ or 0.8, $y = 1.4$, $z = 0.1$)

$$5Cu_{2.3}^{II}Cu_{1.4}^{I}Mo_3O_{12} + 4CuO + 20H_2$$
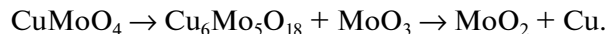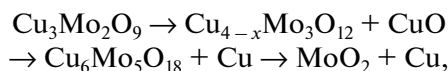$$\rightarrow 3Cu_6Mo_5O_{18} + 4.5Cu + 20H_2O.$$
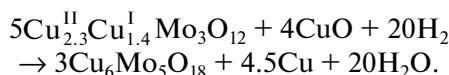
The profile of $CuMoO_4$ reduction by hydrogen can be represented by two peaks of hydrogen consumption: a low-intensity peak with a maximum at 460°C and an intensive peak with a maximum at 491°C (Table 1). The small peak of hydrogen consumption at 460°C is due to the partial reduction of the initial copper(II) molybdate $CuMoO_4$ with the formation of copper(I) molybdate $Cu_6Mo_5O_{18}$ and the segregation of molybdenum(VI) oxide MoO_3:

$$6CuMoO_4 + 3H_2 \rightarrow Cu_6Mo_5O_{18} + MoO_3 + 3H_2O,$$

which was confirmed by the XRD data of the sample reduced to 430°C. The intense peak at 491°C is accompanied by the reduction of the formed mixture of $Cu_6Mo_5O_{18}$ and MoO_3 to metallic Cu and molybdenum(IV) oxide MoO_2:

$$Cu_6Mo_5O_{18} + MoO_3 + 9H_2 \rightarrow 6Cu + 6MoO_2 + 9H_2O.$$
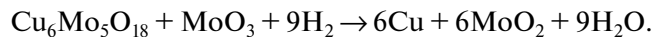
Thereby, according to the results obtained, the reduction of copper molybdates $Cu_3Mo_2O_9$ and $CuMoO_4$ by hydrogen under TPR conditions begins at temperatures below 400°C and is accompanied by a series of consecutive transformations involving the intermediate formation of copper molybdates $Cu_{4-x}Mo_3O_{12}$ and/or $Cu_6Mo_5O_{18}$:

$$Cu_3Mo_2O_9 \rightarrow Cu_{4-x}Mo_3O_{12} + CuO$$
$$\rightarrow Cu_6Mo_5O_{18} + Cu \rightarrow MoO_2 + Cu,$$

$$CuMoO_4 \rightarrow Cu_6Mo_5O_{18} + MoO_3 \rightarrow MoO_2 + Cu.$$

In contrast to [33], the data obtained indicate the phase formation of mixed copper molybdate $Cu_{4-x}Mo_3O_{12}$ as the intermediate reduction product of orthorhombic copper molybdate $Cu_3Mo_2O_9$ to $Cu_6Mo_5O_{18}$. The formation of the mixed copper molybdate $Cu_{4-x}Mo_3O_{12}$ during the $CuMoO_4$ reduction was not observed experimentally, which can be attributed to high rate of its reduction due to the reaction process at higher temperatures as well as to the peculiarities of structural-phase transformations of triclinic copper molybdate.

In general, the reduction of copper and molybdenum in copper molybdates by hydrogen differs from their reduction in individual oxides. In comparison with CuO that is characterized by a one-step hydrogen

reduction of copper(II) to form metallic copper under experimental conditions in the temperature range of 290–350°C, the reduction of copper(II) in copper molybdates occurs consecutively with the intermediate formation of copper(I) and complete reduction to metal at temperatures above 400°C. On the contrary, Mo(VI) in copper molybdates is reduced by hydrogen through one step to form MoO_2 at 350–500°C, while the reduction of the individual molybdenum(VI) oxide under experimental conditions is observed above 600°C and characterized by hydrogen consumption at 725 and 787°C for the temperature range studied, which corresponds, according to [44], to the consecutive reduction of MoO_3 to Mo_4O_{11} and MoO_2. The observed decrease in the reactivity of copper(II) and/or copper(I) and increase in the reactivity of Mo(VI) in copper molybdates as compared to individual oxides strongly depends on the composition and structure of the initial copper molybdate, which can be associated with the stabilization of copper ions in the structure of complex oxides and the activation of molecular hydrogen on the copper particles formed during the reduction followed by the spillover of the active species on copper(I) molybdate, respectively.

Temperature-Programmed Reduction by CO

The TPR-CO profiles for copper molybdates as well as CuO and MoO_3 individual oxides are shown in Fig. 2b. The profile of CuO reduction is characterized by a single intense peak of CO consumption with a maximum at 221°C due to the reduction of copper(II) oxide to metallic copper. The profile of MoO_3 reduction shows a slight CO consumption above 500°C in the form of an unresolved peak due to the beginning of MoO_3 reduction to Mo_4O_{11} [44, 45].

The reduction of both copper molybdates by CO begins at higher temperatures than the reduction of CuO. For both samples, the TPR-CO profiles are characterized by the presence of unresolved peaks of CO consumption, which indicates their partial reduction in the investigated temperature range in comparison with the reduction by hydrogen. Similar to TPR-H_2, the reactivity of copper molybdates $Cu_3Mo_2O_9$ and $CuMoO_4$ is different. The reduction of orthorhombic copper molybdate $Cu_3Mo_2O_9$ is characterized by CO consumption in the range of 280–700°C with peaks at 380 and 542°C. According to the XRD data, a mixture containing mixed copper molybdate $Cu_{4-x}Mo_3O_{12}$, copper(I) molybdate $Cu_6Mo_5O_{18}$ and copper(I) oxide Cu_2O is formed in the course of its reduction within the temperature range studied (Fig. 3a). The composition of products of the CO reduction of $Cu_3Mo_2O_9$ in conjunction with the TPR-CO data indirectly indicates that the formation of mixed copper molybdate $Cu_{4-x}Mo_3O_{12}$ is a consequence of the partial reduction of Cu(II) in it to Cu(I), which agrees with the peak of CO consumption at 380°C. The formation of $Cu_{4-x}Mo_3O_{12}$

and its subsequent reduction to $Cu_6Mo_5O_{18}$ seems to be accompanied by the segregation of copper excess in the form of CuO quickly reducing to Cu_2O, which agrees with the peak of CO consumption at 542°C.

As for TPR-H_2, the reduction of $CuMoO_4$ by CO is observed at much higher temperatures than the reduction of $Cu_3Mo_2O_9$. The corresponding profile of the reduction is characterized by CO consumption in the range of 460–700°C with maxima at 521 and 551°C. According to the XRD data, the copper molybdate $CuMoO_4$ reduces in the temperature range studied to form a mixture including mixed copper molybdate $Cu_{4-x}Mo_3O_{12}$, copper(I) molybdates with different composition – $Cu_6Mo_5O_{18}$ and $Cu_4Mo_5O_{17}$ and also molybdenum oxides MoO_2 and Mo_4O_{11} (Fig. 3b). The composition of products of $CuMoO_4$ reduction indirectly indicates that its reduction occurs through the intermediate formation of the mixed copper molybdate $Cu_{4-x}Mo_3O_{12}$ with the segregation of molybdenum excess in the form of MoO_3 followed by formation of copper(I) molybdates $Cu_6Mo_5O_{18}$ and $Cu_4Mo_5O_{17}$. Considering the absence of copper oxide and metallic copper phases in the final products, the presence of Mo_4O_{11} and MoO_2 in the products can be associated both with the reduction of MoO_3 and partial reduction of $Cu_4Mo_5O_{17}$ to form an additional amount of $Cu_6Mo_5O_{18}$.

Therefore, the TPR-CO data indicates that the reduction of both copper(II) molybdates occurs through the intermediate formation of the mixed copper molybdate $Cu_{4-x}Mo_3O_{12}$, and that the reactivity of copper(II) and/or copper(I) in copper molybdates decreases as compared with the individual copper oxide due to the stabilization of copper ions in the structure of complex oxides. However, in contrast to TPR-H_2, an increase in the reactivity of Mo(VI) in copper molybdates was not observed as compared to that of the individual molybdenum(VI) oxide. This confirms that in case of hydrogen reduction the activation of molecular hydrogen takes place on the metallic copper particles formed during the reduction followed by the active particle transfer to copper(I) molybdate contributing to its further reduction.

Temperature-Programmed Reduction by Carbon

The TPR-C profiles of simple and complex oxides of copper and molybdenum are shown in Fig. 4. In contrast to reduction by hydrogen and CO, the carbon reduction of individual CuO and MoO_3 oxides as well as copper molybdates occurs in the close temperature ranges above 400°C under similar experimental conditions (heating rate of 5°C/min) (Fig. 4a). The reduction of CuO occurs in the temperature range of 400–700°C and is characterized on the TPR-C profile by the two peaks of CO_2 evolution with maxima at 491 and 644°C corresponding to the sequential formation of Cu_2O and Cu, which correlates with the literature
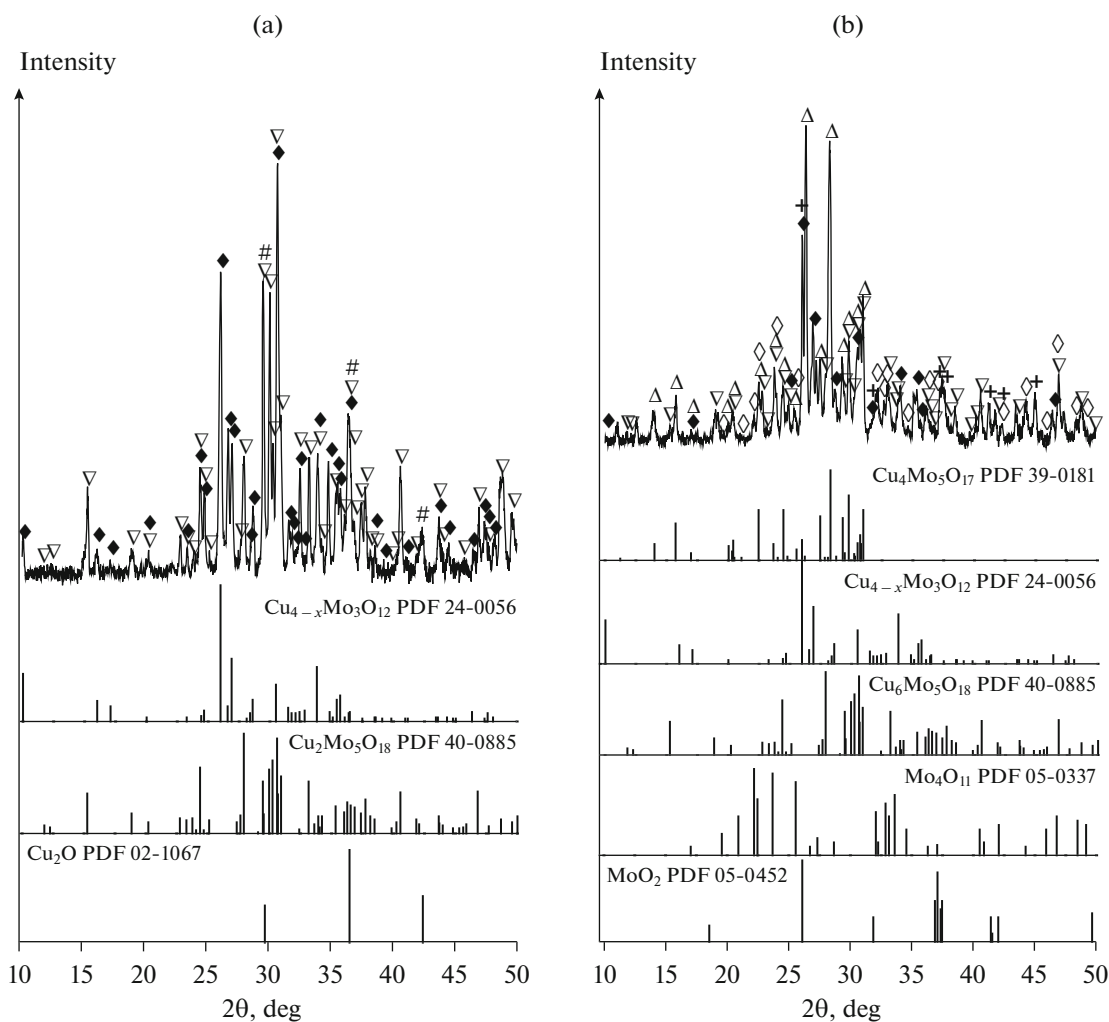
(a)

(b)

Fig. 3. XRD patterns of $Cu_3Mo_2O_9$ (a) and $CuMoO_4$ (b) samples reduced during TPR-CO, as well as line-diagrams of phases identified (($+$) MoO_2, ($\triangledown$) $Cu_6Mo_5O_{18}$, ($\blacklozenge$) $Cu_{4-x}Mo_3O_{12}$, ($\triangle$) $Cu_4Mo_5O_{17}$, ($\lozenge$) Mo_4O_{11}, ($\#$) Cu_2O).

data [26, 46]. There is an asymmetric peak of CO_2 evolution with a maximum at 601°C in the temperature range of 550−710°C in the TPR-C profile of MoO_3, which is caused by the reduction of the initial oxide to form MoO_2. The carbon reduction of orthorhombic copper molybdate $Cu_3Mo_2O_9$ begins at 425°C under experimental conditions and is characterized by the intense peak of CO_2 evolution with a maximum at 480°C and a shoulder at 503°C, smaller intense peak with a maximum at 584°C, and also wide unresolved peak at higher temperatures at the TPR-C profile. The reduction of triclinic copper molybdate $CuMoO_4$ begins at 406°C and is characterized by two peaks of CO_2 evolution with maxima at 471 and 560°C, and a weak CO_2 evolution at higher temperatures.

The presence of several peaks in the TPR-C profiles of the samples indicates the consecutive reduction of copper molybdates similar to reducing by other agents. According to the XRD data, the CO_2 evolution

during the reduction of $Cu_3Mo_2O_9$ in the range of 430−530°C is caused by the reduction of Cu(II) to Cu(I) accompanied by the consecutive formation of $Cu_{4-x}Mo_3O_{12}$ and $Cu_6Mo_5O_{18}$ and segregation of copper excess in the form of Cu_2O (or CuO, rapidly reducing to Cu_2O) (Fig. 5a). The further reduction of the sample in the studied temperature range results in the formation of a mixture containing significant amounts of $Cu_6Mo_5O_{18}$, MoO_2 and Cu, as well as the admixture of Cu_2O.

According to XRD, the reduction of $CuMoO_4$ at the range of 425−500°C is accompanied by the formation of a mixture of copper(I) molybdates $Cu_6Mo_5O_{18}$ and $Cu_4Mo_5O_{17}$ (Fig. 5b). The formation of mixed copper molybdate $Cu_{4-x}Mo_3O_{12}$ in the course of $CuMoO_4$ reduction was not reliably confirmed by off line XRD, but the presence of seral overlapped peaks in the range 425−500°C in the TPR-C profile does not exclude its formation before formation of cop-

per(I) molybdates. The further temperature increase in the range of $500-600°C$ results in the primary reduction of $Cu_4Mo_5O_{17}$ to Cu and MoO_2. The reduction of $Cu_6Mo_5O_{18}$ with formation of Cu and MoO_2 is observed above $550°C$ and does not occur completely in the investigated temperature range.

Generally, the copper oxide CuO and the initial copper molybdates $CuMoO_4$ and $Cu_3Mo_2O_9$ show a comparable reactivity towards interaction with carbon to form Cu(I) under the experimental conditions. In contrast to the interaction with H_2 and CO, the absence of significant differences in the reactivity of the initial compounds towards carbon seems to be caused by the peculiarities of heterogeneous reactions between solids, which are limited by the transfer of components to the reaction zone. The observed effect can be related to the induction period of the interaction of initial compounds and soot under TPR-C conditions due to a set of initial changes in the system (covering one component with others through the surface diffusion or sublimation, particle reorientations) as well as with a low rate of bulk diffusion of atoms of the components at the temperatures considered. The increase of the heating rate during the TPR-C (Fig. 4b) leads to a shift in the profiles of the copper molybdates reduction to the high-temperature region without a significant change in the form of the curve, which makes the differences in their reactivity more noticeable. Similar to their reduction by hydrogen and CO, the reduction of orthorhombic copper molybdate $Cu_3Mo_2O_9$ by carbon with the formation of copper(I) molybdates occurs at lower temperatures than those of the trigonal copper molybdate $CuMoO_4$.

At the same time, the depth of Cu(I) reduction to Cu and Mo(VI) reduction to Mo(IV) in the samples is different independently on heating rate in the investigated temperature range and is determined by the reactivity of the intermediate products − copper(I) molybdates $Cu_4Mo_5O_{17}$ and $Cu_6Mo_5O_{18}$. Copper molybdate $Cu_6Mo_5O_{18}$ demonstrates relatively low reactivity towards carbon, while copper molybdate $Cu_4Mo_5O_{17}$ is characterized by a higher reactivity in comparison with the individual oxides. The observed differences in the reactivity of the initial and formed copper molybdates can be connected with the different crystallochemical mechanisms of the reduction of Cu(I) molybdates, which may be due to the difference in their structure, mobility of individual atoms in the lattice, etc.

Generalizing the results of the phase and structural transformations of the mixed molybdenium and copper oxides $Cu_3Mo_2O_9$ and $CuMoO_4$ interaction with different reactants, it is noteworthy that their reduction accompanied by a series of consecutiv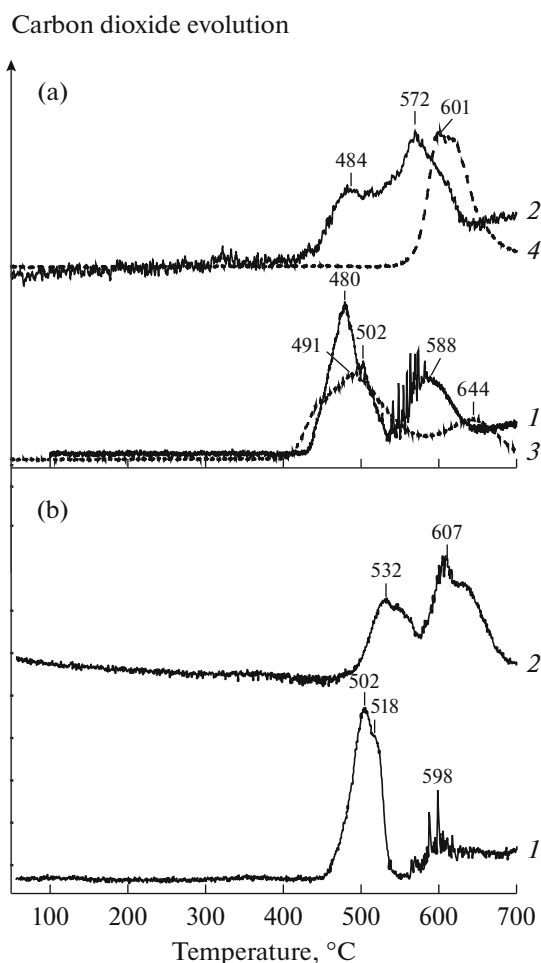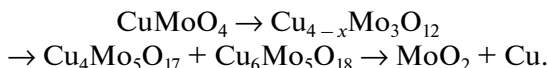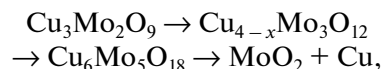e transformations, normally including the intermediate formation of copper molybdates $Cu_{4-x}Mo_3O_{12}$, $Cu_6Mo_5O_{18}$ and/or $Cu_4Mo_5O_{17}$:

$$Cu_3Mo_2O_9 \rightarrow Cu_{4-x}Mo_3O_{12}$$
$$\rightarrow Cu_6Mo_5O_{18} \rightarrow MoO_2 + Cu,$$

$$CuMoO_4 \rightarrow Cu_{4-x}Mo_3O_{12}$$
$$\rightarrow Cu_4Mo_5O_{17} + Cu_6Mo_5O_{18} \rightarrow MoO_2 + Cu.$$

The non-stoichiometric excess of copper or molybdenum in the course of such transformations segregates as CuO and MoO_3, which can be further reduced to Cu_2O, Cu and Mo_4O_{11}, MoO_2, respectively. The depth of the reduction of initial copper molybdates and the rate of the individual steps depend appreciably on the composition and structure of the initial and intermediate copper molybdates as well as on the nature of the reducing agent determining the catalytic properties of the samples on the basis thereof and giving grounds for a purposeful control of the system state. As an example, catalytic properties of copper molybdates with different compositions of $Cu_3Mo_2O_9$ and $CuMoO_4$ were
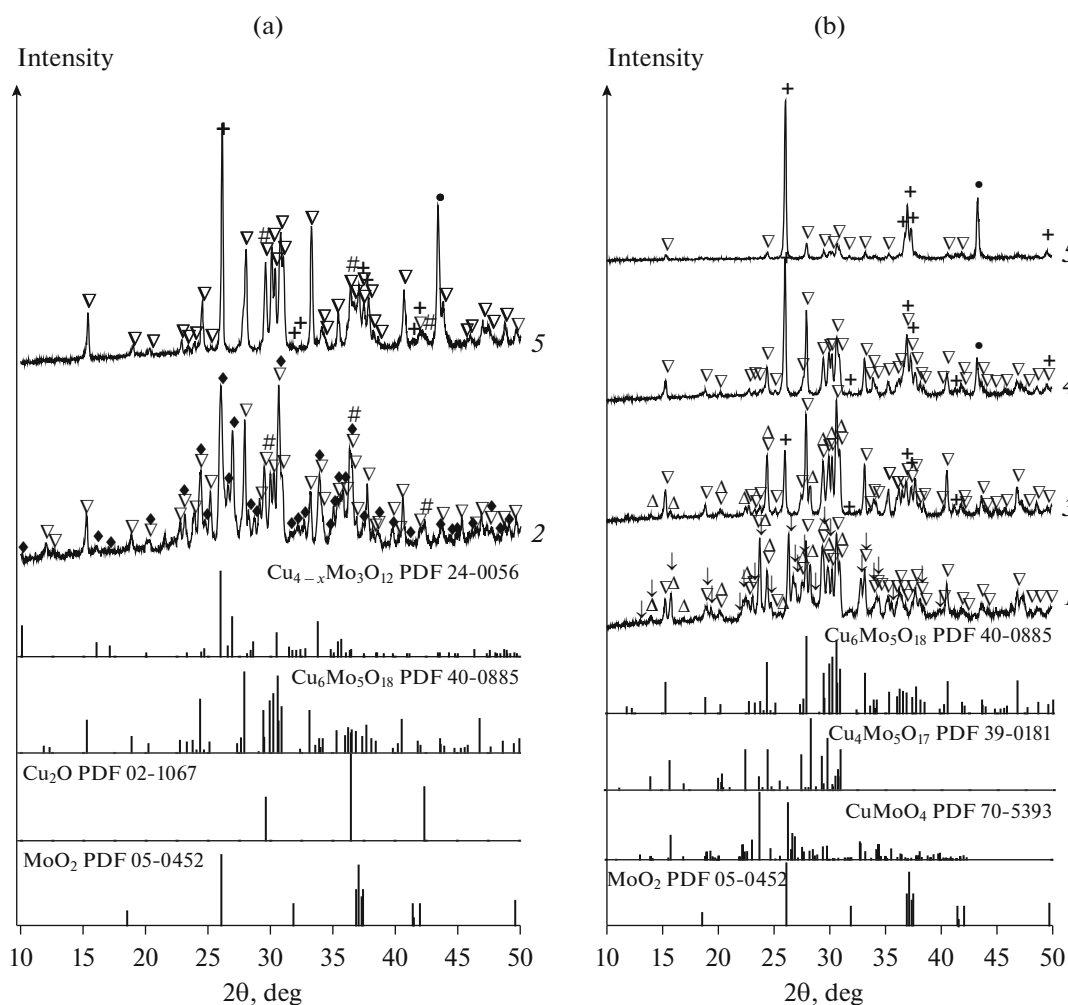
Carbon dioxide evolution

Fig. 4. The TPR-C profiles of $Cu_3Mo_2O_9$ (*1*), $CuMoO_4$ (*2*), CuO (*3*), MoO_3 (*4*) samples obtained at heating rate of 5 (a) and 10°C/min (b).

Fig. 5. X-ray patterns of $Cu_3Mo_2O_9$ (a) and $CuMoO_4$ (b) samples reduced during TPR-C to 494 (*1*), 500 (*2*), 538 (*3*), 575 (*4*) and 700°C (*5*), and also line-diagrams of phases identified (($\bullet$) Cu, (+) MoO_2, ($\triangledown$) $Cu_6Mo_5O_{18}$, ($\blacklozenge$) $Cu_{4-x}Mo_3O_{12}$, ($\triangle$) $Cu_4Mo_5O_{17}$, ($\diamond$) Mo_4O_{11}, (#) Cu_2O).

studied in the model reactions of CO and soot oxidation.

Investigation of Catalytic Properties

The dependence of CO conversion as well as the rate of CO oxidation on temperature for $Cu_3Mo_2O_9$ and $CuMoO_4$ samples are shown in Fig. 6. For $Cu_3Mo_2O_9$, the CO oxidation begins at 300°C and its rate significantly rises with the temperature increase. The complete CO conversion is achieved at 500°C. The second CO oxidation on this sample has shown a reproducible result. For $CuMoO_4$, the noticeable CO oxidation begins at temperatures above 450°C.

According to current understanding the catalytic activity of copper-oxide catalysts in the CO oxidation is caused by the formation of Cu(I) surface sites under catalytic conditions [47−49]. The relatively high catalytic activity of $Cu_3Mo_2O_9$ towards CO oxidation correlates well with the possible formation of copper(I) compounds, according to the TPR-CO data, in particular $Cu_{4-x}Mo_3O_{12}$, under reactive atmosphere at temperatures above 280°C. The compounds formed can be both bulk and surface phases. In general, the catalytic activity of the sample based on orthorhombic copper molybdate $Cu_3Mo_2O_9$ towards CO oxidation is not very high in comparison with such catalysts as Ag/SiO_2 and Pd/CeO_2 [50, 51]. This indicates the formation of centers of selective oxidation in it, but not those of deep oxidation, which are attractive for the partial oxidation of organic compounds [52, 53].

In case of copper molybdate $CuMoO_4$, the formation of copper(I) compounds occurs at temperatures above 450°C under the TPR-CO conditions, which also correlates with the absence of its catalytic activity towards CO oxidation at lower temperatures under the reaction conditions.
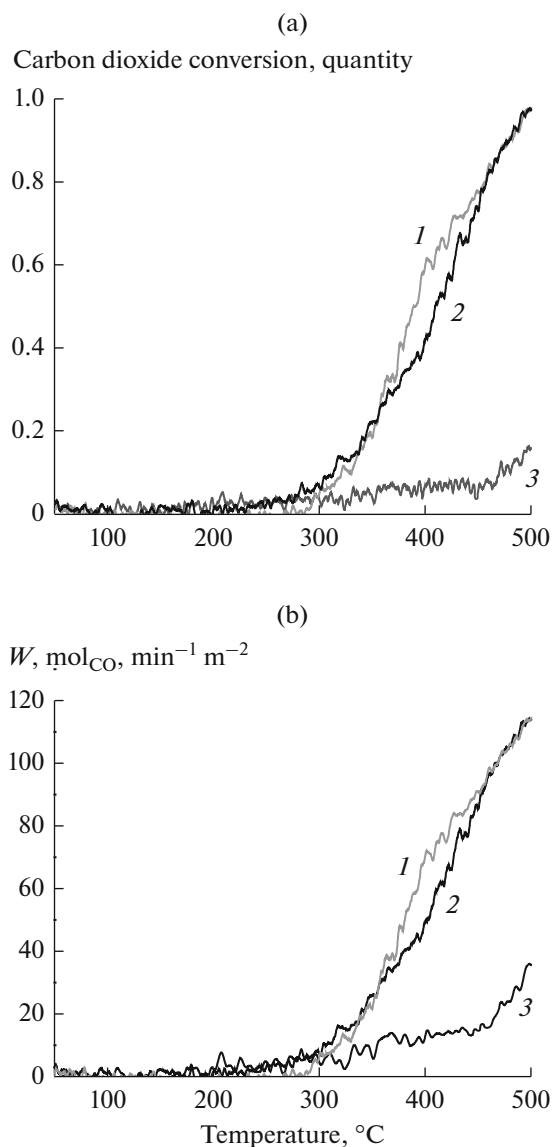
(a)

Carbon dioxide conversion, quantity

(b)

W, $\mathrm{mol_{CO}}$, $\mathrm{min^{-1}}$ $\mathrm{m^{-2}}$

Fig. 6. The temperature dependences of CO conversion (a) and CO oxidation rate (b) for $Cu_3Mo_2O_9$ (*1*, *2*) and $CuMoO_4$ (*3*): (*1*) CO oxidation on a fresh sample, (*2*) reusing of catalyst.

Fig. 7. TG-curves (a) and mass spectrometric analysis data (b) of soot oxidation gaseous products under different conditions: (*1*) the non-catalytic oxidation, (*2*) $Cu_3Mo_2O_9$ catalyst, (*3*) $CuMoO_4$ catalyst.

The results of the study of catalytic properties of $Cu_3Mo_2O_9$ and $CuMoO_4$ in soot oxidation are shown in Fig. 7. Non-catalytic soot combustion occurs in the temperature range of 550−700°C with a maximum oxidation rate at 670°C (Figs. 6a, 6b). The temperature of soot oxidation in the presence of copper molybdates $Cu_3Mo_2O_9$ and $CuMoO_4$ appreciably decreases, which correlates with the literature data [21, 22]. In contrast to CO oxidation, the soot oxidation in the presence of copper molybdates of various compositions occurs in the same temperature range of 400−600°C.

In all cases, the soot combustion occurs with the formation of CO_2, the evolution of CO (according to
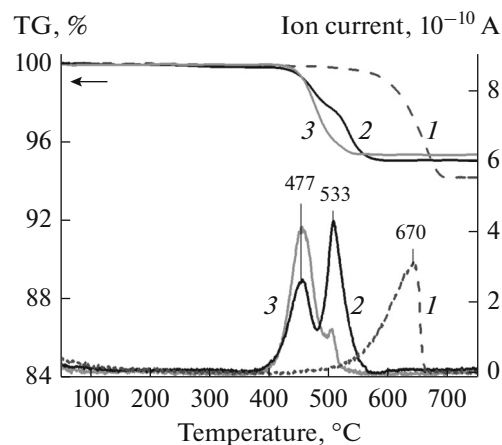
the mass-spectrometric analysis of gaseous products, when He was used as an inert diluent) is not observed. The soot oxidation occurs on $Cu_3Mo_2O_9$ at 477 and 533°C. The soot oxidation over $CuMoO_4$ is also accompanied by the appearance of two peaks of CO_2 evolution at closed temperatures: an intensive peak at 477°C and a small one at 528°C.

The presence of two peaks of CO_2 evolution in the TPR-C profiles corresponding to two peaks in the DTG curves is a reproducible result (Fig. 8). This was attributed to the phase-structural transformations of copper molybdates under the reactive atmosphere. Similar to [22, 23], the first peak of CO_2 evolution is related to the soot combustion in the presence of mixed copper molybdate $Cu_{4-x}Mo_3O_{12}$, which, according to the present studies, is the product of the partial reduction of initial $CuMoO_4$ and $Cu_3Mo_2O_9$. The appearance of the second peak is explained by deeper conversion of copper molybdates under the reactive atmosphere, particularly by the formation of the $Cu_6Mo_5O_{18}$, characterized with its own catalytic activity. This correlates with the obtained results of TPR-C under experimental conditions comparable to the conditions of catalytic studies (heating rate of 10°C/min, flow rate of 20 mL/min) (Fig. 8). Thus, the beginning of the soot oxidation by gas oxygen on $Cu_3Mo_2O_9$ coincides with the beginning of consecutive sample reduction to $Cu_{4-x}Mo_3O_{12}$ and $Cu_6Mo_5O_{18}$ under the TPR-C conditions in the range of 450−550°C. The appearance of the second peak of CO_2 evolution accords with the possibility of $Cu_6Mo_5O_{18}$ formation under the TPR-C conditions. According to the obtained results, the amount of CO_2 evolved due to the catalytic CO oxidation is much lower than the amount of gas oxygen reacted. This also indicates that the soot oxidation is directly connected with the
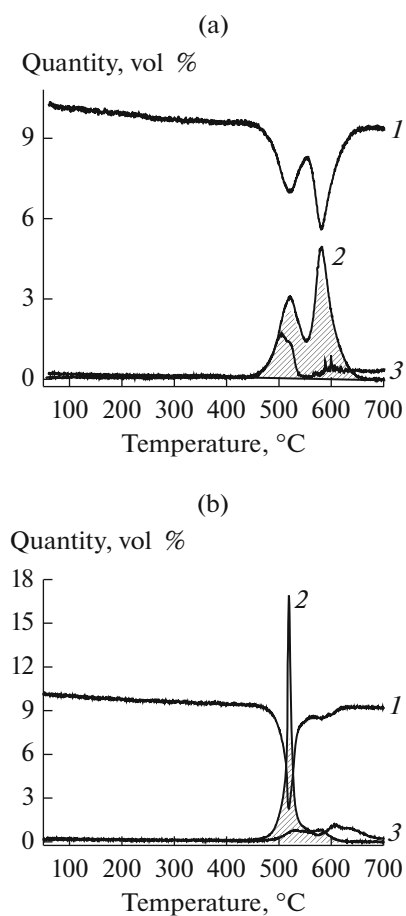
(a)

Quantity, vol %

(b)

Quantity, vol %

Fig. 8. Temperature dependences of the oxygen (*1*) and CO_2 (*2*) amounts, respectively, consumed and evolved during the catalytic CO oxidation, and the amount of CO_2 (*3*) evolved during TPR-C on $Cu_3Mo_2O_9$ (a) and $CuMoO_4$ (b) samples under comparable experimental conditions (heating rate 10°C/min, flow rate 20 mL/min). The shaded areas show the amount of CO_2 conforming to the amount of oxygen consumed from the gas phase.

reduction of the initial copper molybdate, which, at least at the beginning, occurs on the surface.

For $CuMoO_4$, the CO oxidation starts slightly before its bulk reduction under the TPR-C conditions. This indicates the surface reduction of the initial molybdate in the beginning. However, when the temperature of the $CuMoO_4$ reduction to copper(I) compounds under TPR-C conditions is achieved, a sharp increase in the rates of CO_2 evolution and oxygen consumption is observed under the catalytic reaction conditions, with the amount of evaluated CO_2 being significantly outweigh that of gas oxygen consumed. Further temperature increase is accompanied by a synchronous change in the rates of CO_2 evolution and oxygen consumption, and stoichiometric changes of CO_2 and O_2 amounts. This indicates the reduction of the initial copper(II) molybdate with the sequential formation of at least two catalytically active phases

during the reaction. The made assumptions undoubtedly require additional studies, including in situ methods.

In general, the results of the present study indicate that the phase and structural transformations of copper molybdates under the reaction medium, particularly the formation of $Cu_{4-x}Mo_3O_{12}$ and $Cu_6Mo_5O_{18}$ phases, have a significant impact on the formation of the active state of the copper molybdate-based catalysts in the studied model reactions.

ACKNOWLEDGMENTS

REFERENCES

1. Chub, O.V., Mokrinskii, V.V., Reshetnikov, S.I., Yazykov, N.A., Dubinin, Yu.V., Simonov, A.D., and Yakovlev, V.A., *Katal. Prom-sti*, 2013, no. 5, p. 54.
2. Toniolo, F.S., Barbosa-Coutinho, E., Schwaab, M., Leocadio, I.C., Aderne, R.S., Schmal, M., and Pinto, J.C., *Appl. Catal. A*, 2008, vol. 342, no. 1, p. 87.
3. Mei, C., Yuan, Y., Li, X., and Mei, D., *Bull. Chem. React. Eng. Catal.*, 2016, vol. 11, no. 3, p. 389.
4. Wang, J. Cheng, L., An, W., Xu, J., and Men, Y., *Catal. Sci. Technol.*, 2016, vol. 6, no. 19, p. 7342.
5. Leocadio, I.C.L., Braun, S., and Schmal, M., *J. Catal.*, 2004, vol. 223, no. 1, p. 114.
6. Wang, C.H. and Weng, H.S., *Ind. Eng. Chem. Res.*, 1997, vol. 36, no. 7, p. 2537.
7. Li, L., Mao, D., Yu, J., and Guo, X., *J. Power Sources*, 2015, vol. 279, p. 394.
8. Pham, T.T.P., Nguyen, P.H.D., Vo, T.T., Luu, C.L., and Nguyen, H.H.P., *Mater. Chem. Phys.*, 2016, vol. 184, p. 5.
9. Rousseau, R., Dixon, D.A., Kay, B.D., and Dohnalek, Z., *Chem. Soc. Rev.*, 2014, vol. 43, no. 22, p. 7664.
10. Gordeev, A.V., Zhukov, I.A., Gordeeva, O.S., Pavlitskii, N.A., Merk, A.A., Soltys, E.V., and Knyazev, A.S., *Izv. Vyssh. Uchebn. Zaved., Khim. Khim. Tekhnol., Ser. Fizika*, 2011, no. 12/2, p. 15.
11. Amakawa, K., Krohnert, J., Wrabetz, S., Frank, B., Hemmann, F., Jager, C., Schlogl, R., and Trunschke, A., *ChemCatChem*, 2015, vol. 7, no. 24, p. 4059.
12. US Patent no. 20160075617, 2016.
13. Boyadjian, C., van der Veer, B., Babich, I.V., Lefferts, L., and Seshan, K., *Catal. Today*, 2010, vol. 157, no. 1, p. 345.
14. Al-Yassir, N. and Le Van Mao, R., *Appl. Catal. A*, 2006, vol. 305, no. 2, p. 130.
15. Choudhary, V.R., Jha, R., Chaudhari, N.K., and Jana, P., *Catal. Commun.*, 2007, vol. 8, no. 10, p. 1556.
16. Choudhary, V.R., Jha, R., and Jana, P., *Catal. Commun.*, 2008, vol. 10, no. 2, p. 205.
17. Wang, C.H., Lee, C.N., and Weng, H.S., *Ind. Eng. Chem. Res.*, 1998, vol. 37, p. 1774.
18. Wang, C.H., Lin, S.S., Liou, S.B., and Weng, H.S., *Chemosphere*, 2002, vol. 49, no. 4, p. 389.

19. Dong, L., Yao, X., and Chen, Y., *Chin. J. Catal.*, 2013, vol. 34, no. 5, p. 851.

20. Devulapelli, V.G. and Sahle-Demessie, E., *Appl. Catal. A*, 2008, vol. 348, p. 86.

21. Chu, W.G., Wang, H.F., Guo, Y.J., Zhang, L.N., Han, Z.H., Li, Q.Q., and Fan, S.S., *Inorg. Chem.*, 2009, vol. 48, no. 3, p. 1243.

22. Lebukhova, N.V., Karpovich, N.F., Makarevich, K.S., and Chigrin, P.G., *Kataliz v Prom-sti*, 2008, no. 6, p. 35.

23. Chigrin, P.G., Lebukhova, N.V., and Ustinov, A.Yu., *Kinet. Katal.*, 2013, vol. 54, no. 1, p. 79.

24. Hasan, M.A., Zaki, M.I., Kumari, K., and Pasupulety, L., *Thermochim. Acta*, 1998, vol. 320, no. 1, p. 23.

25. Chigrin, P.G., *Cand. Sci. (Chem.) Dissertation*, Vladivostok: DVO RAN, 2012.

26. Lebukhova, N.V. and Karpovich, N.F., *Neorg. Mater.*, 2008, vol. 44, no. 8, p. 1003.

27. Bettahar, M.M., Costentin, G., Savary, L., and Lavalley, J.C., *Appl. Catal. A*, 1996, vol. 145, no. 1, p. 1.

28. Habbr, J., Stoch, J., and Siltowski, T., *Stud. Surf. Sci. Catal.*, 1981, vol. 7, p. 1402.

29. Moro-Oka, Y., Takita, Y., and Ozaki, A., *J. Catal.*, 1971, vol. 23, no. 2, p. 183.

30. Haber, J. and Wiltowski, T., *Bull. Acad. Pol. Sci., Ser. Sci. Chim.*, 1979, vol. 27, p. 785.

31. Maggiore, R., Galvagno, S., Bart, J.C.J., Giannetto, A., and Toscano, G., *Z. Phys. Chem.*, 1982, vol. 132, p. 85.

32. Wen, W., Jing, L., White, M.G., Marinkovic, N., Hanson, J.C., and Rodriguez, J.A., *Catal. Lett.*, 2007, vol. 113, nos. 1−2, p. 1.

33. Machej, T. and Ziolkowski, J., *J. Solid State Chem.*, 1980, vol. 31, no. 2, p. 145.

34. Koop, M. and Müller-Buschbaum, Hk., *Z. Anorg. Allg. Chem.*, 1985, vol. 531, no. 12, p. 140.

35. Benchikhi, M., El Ouatib, R., Guillemet-Fritsch, S., Chane-Ching, J.Y., Er-Rakho, L., and Durand, B., *Ceram. Int.*, 2014, vol. 40, no. 4, p. 5371.

36. Asano, T., Nishimura, T., Ichimura, S., Inagaki, Y., Kawae, T., Fukui, T., and Gaulin, D.B., *J. Phys. Soc. Jpn.*, 2011, vol. 80, no. 9.

37. Kihlborg, L., Norrestam, R., and Olivecrona, B., *Acta Crystallogr.*, 1971, vol. 27, no. 11, p. 2066.

38. Vilminot, S., Andre, G., and Kurmoo, M., *Inorg. Chem.*, 2009, vol. 48, no. 6, p. 2687.

39. Raw, A.D., Ibers, J.A., and Poeppelmeier, K.R., *J. Solid State Chem.*, 2013, vol. 200, p. 165.

40. Katz, L., Kasenally, A., and Kihlborg, L., *Acta Crystallogr.*, 1971, vol. 27, no. 11, p. 2071.

41. Steiner, U., Reichelt, W., and Oppermann, H., *Z. Anorg. Allg. Chem.*, 1996, vol. 622, no. 8, p. 1428.

42. Haber, J., Machej, T., Ungier, L., and Ziolkowski, J., *J. Solid State Chem.*, 1978, vol. 25, no. 3, p. 207.

43. Machej, T. and Ziolkowski, J., *J. Solid State Chem.*, 1980, vol. 31, no. 2, p. 135.

44. Schulmeyer, W.V. and Ortner, H.M., *Int. J. Refract. Met. Hard Mater.*, 2002, vol. 20, no. 4, p. 261.

45. Samsuri, A., Saharuddin, T.S.T., Salleh, F., Othaman, R., Hisham, M.W.M., and Yarmo, M.A., *Malaysian J. Anal. Sci.*, 2016, vol. 20, no. 2, p. 382.

46. Kirakosyan, H., Minasyan, T., Niazyan, O., Aydinyan, S., and Kharatyan, S., *J. Therm. Anal. Calorim.*, 2016, vol. 123, no. 1, p. 35.

47. Wang, X., Hanson, J.C., Frenkel, A.I., Kim, J.Y., and Rodriguez, J.A., *J. Phys. Chem. B*, vol. 108, no. 36, p. 13667.

48. Yang, B.X., Ye, L.P., Gu, H.J., Huang, J.H., Li, H.Y., and Luo, Y., *J. Mol. Model*, 2015, vol. 21, no. 8, p. 195.

49. Svintsitskiy, D.A., Kardash, T.Y., Stonkus, O.A., Slavinskaya, E.M., Stadnichenko, A.I., Koscheev, S.V., and Boronin, A.I., *J. Phys. Chem.*, 2013, vol. 117, no. 28, p. 14588.

50. Dutov, V.V., Mamontov, G.V., Zaikovskii, V.I., and Vodyankina, O.V., *Catal. Today*, 2016, vol. 278, p. 150.

51. Slavinskaya, E.M., Kardash, T.Yu., Stonkus, O.A., Gulyaev, R.V., Lapin, I.N., Svetlichnyi, V.A., and Boronin, A.I., *Catal. Sci. Technol.*, 2016, vol. 6, p. 6650.

52. Huang, W., Sun, G., and Cao, T., *Chem. Soc. Rev.*, 2017, vol. 46, p. 1977.

53. Zhang, Q., Deng, W., and Wang, Y., *Chem. Commun.*, 2011, vol. 47, p. 9275.